Journal Pre-proofs

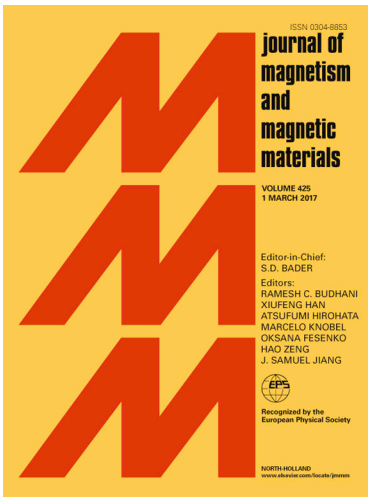

Research articles

Thermal assisted tailoring of magnetic coercivity in Iron thin films on unstable Lithium Niobate substrate

V. Polewczyk, G. Vinai, F. Motti, S. Santhosh, S. Benedetti, G. Rossi, P. Torelli

PII: S0304-8853(20)31024-6
DOI: https://doi.org/10.1016/j.jmmm.2020.167257
Reference: MAGMA 167257

To appear in: *Journal of Magnetism and Magnetic Materials*

Received Date: 9 April 2020
Revised Date: 21 July 2020
Accepted Date: 21 July 2020

Please cite this article as: V. Polewczyk, G. Vinai, F. Motti, S. Santhosh, S. Benedetti, G. Rossi, P. Torelli, Thermal assisted tailoring of magnetic coercivity in Iron thin films on unstable Lithium Niobate substrate, *Journal of Magnetism and Magnetic Materials* (2020), doi: https://doi.org/10.1016/j.jmmm.2020.167257

Thermal assisted tailoring of magnetic coercivity in Iron thin films on unstable Lithium Niobate substrate

V. Polewczyk,[1] G. Vinai,[1] F. Motti,[1,2] S. Santhosh,[1] S. Benedetti,[3] G. Rossi[1,2] and P. Torelli[1]

[1] Istituto Officina dei Materiali (IOM)–CNR, Laboratorio TASC, Area Science Park, S.S.14, km 163.5, I-34149 Trieste, Italy
[2] Dipartimento di Fisica, Università degli Studi di Milano, Via Celoria 16, I-20133, Milano, Italy
[3] Istituto Nanoscienze-CNR, via Campi 213/a,41125, Modena, Italy
E-mail: polewczyk@iom.cnr.it

Abstract

In this work, we present an investigation on the effects of thermal annealing on the magnetic response of Lithium Niobate/Fe samples. Fe thin films have been deposited on Lithium Niobate Z-cut ferroelectric substrates by vapor phase epitaxy. A series of annealing treatments were performed on the samples, monitoring the evolution of their magnetic properties, both at the surface and on the volume. The combination of structural, magnetic, chemical and morphological characterizations shows that the modification of the chemical properties, *i.e.* the phase decomposition, of the substrate upon annealing affects drastically the magnetic behavior of the interfacial Fe layer. By tuning the annealing temperature, the magnetic coercive field value can be increased by an order of magnitude compared to the as-grown value, keeping the same in-plane isotropic behavior. Since no evident differences were recorded in the Fe layer from the chemical point of view, we attribute the origin of this effect to an intermixing process between a fragment of the substrate and the Fe thin film upon critical temperature annealing, process that is also is responsible for the observed changes in roughness and morphology of the magnetic thin film.

Keywords: Lithium Niobate, Ferroelectric substrate, Iron, As-grown, Annealing, Intermixing, Coercive field.

1. Introduction

The control of magnetization and magnetic anisotropy are of utmost importance in spintronics, especially in view of applications for data storage and data manipulation. Tuning of the magnetic properties of an heterostructure can be pursued in several ways. One way is tailoring the magnetic film overlayer by multi-stack architecture [1, 2] or exploring different deposition conditions (rate, substrate temperature, angle of impact of the atomic beams on the substrates) [3, 4]. A second way is to act on the substrate to induce changes in the epitaxial magnetic overlayer, as for example by exploiting interface stress control of piezoelectric substrates [5-9] or by controlled after-growth annealing. In this last case, magnetocrystalline anisotropy of a ferromagnetic overlayer may be induced by structural anisotropy at the interface driven by the substrate surface crystallography [10, 11]. Thermal annealing may as well affect the substrate structure and composition. This is particularly relevant in the case of unstable substrates. Among them, ferroelectric Lithium Niobate $LiNbO_3$ (LN) is a paradigmatic case. Its properties strongly depend on the quality of its synthesis, *i.e.* its composition (stoichiometric, congruent, etc. [12]). In fact, ions tend to migrate easily during crystal growth, creating intrinsic defects in the crystal lattice [13-15]. LN crystals are extremely useful in ferroelectric-piezoelectric based devices [16, 17]. Being LN insulating, a conductive amorphous, polycrystalline or epitaxial layer is often deposited on top of it to act as electrode [18-23]. Patterned ferromagnetic layers can be used as sensors of magnetic surface acoustic waves, being especially efficient at room temperature [18, 24, 25]. The performances of such devices deteriorate above 300°C because of LN becoming chemically unstable [26, 27]. This is mostly due to a dissociation reaction that occur in the substrate, which leads to a combination of effects such as surface rearrangement, increase of surface roughness and/or changes in the surface stoichiometry [27]. Such changes in the substrate are reflected in changes of the overgrown materials that can experience oxidation and/or modifications of their properties.

In this work, we combined structural, magnetic, chemical and morphological analysis to investigate how the chemical modifications of LN upon annealing in the temperature range from 300 to 800°C induce giant changes on the magnetic properties of a Fe thin film grown on top of it.

By performing magneto-optic Kerr effect (MOKE), X-Ray Diffraction (XRD), X-ray Photoemission Spectroscopy (XPS), X-ray Absorption Spectroscopy (XAS), Atomic Force Microscopy (AFM) and Energy-Dispersive X-ray spectroscopy (EDS), we characterize the substantial magnetic changes that occur in the system. These changes are not related to variations in the chemical properties of the magnetic layer, but they are mostly due to Fe microstructural/morphological variations induced by Li and Nb oxides clusters interdiffusion towards the surface after phase decomposition.

2. Fe thin film depositions and thermal post-treatments

Black LN substrates Z-cut, *i.e.* orientated with the hexagonal lattice c-axis perpendicular to the surface, were cleaned with acetone and ethanol in an ultrasonic bath, with outgassing in air at 80°C for 30 minutes before inserting in the Ultra High Vacuum (UHV) apparatus.

10 nm Fe thin films were deposited on it by vapor phase epitaxy at a pressure not exceeding 1.10^{-9} mbar and on the substrate maintained at Room Temperature (RT). Shadowing effects [28] were avoided by orienting the sample surface perpendicularly to the metal vapor beam average direction during the deposition. Multiple samples were deposited at different deposition rates in the [1 - 4 Å.min^{-1}] range, as calibrated by quartz microbalance. Different deposition rates in this range did not affect the results. All the presented results refer to Iron samples grown at the rate of 2 Å.min^{-1}.

Fe (a = b = c = 0.286 nm) generally grows cubic with a closed packed (110) bcc planar film, but LN has a hexagonal unit cell (a = b = 0.5149 nm and c = 1.386 nm) [19]. The lattice mismatch between substrate and overlayer is large and a deposition at room temperature is expected to give a disordered polycrystalline growth of Fe on top of LN. This was confirmed by the lack of X-ray diffraction peaks or ion electron-diffraction spots in LEED (not reported here).

After deposition, different annealing in UHV condition were done by Joule heating and electron bombardment, using a filament placed below the sample holder, at temperatures ranging from 300 to 800°C for one hour.

The effects of the thermal treatments on the LN substrate and Iron overlayer were probed by XRD with a PanAnalytical X'Pert Pro diffractometer (Cu-K_α wavelength) in high intensity mode, *i.e.* using a Parallel Plate Collimator (PPC) as secondary optical block. The pristine sample shows only the peak corresponding to the LN substrate (Figure 1) while no peaks associated to the Fe overlayer were observed. For all the annealing temperatures, no Fe crystallization, *i.e.* single crystal domain, was observed neither by LEED nor by XRD. On the other hand, LN substrate present a structural change after annealing at 800°C, with the appearance of a new phase, as shown in Figure 1.

Together with the substrate diffraction peak of $LiNbO_3$ (0006), a new crystalline phase, *i.e.* $LiNb_3O_8$ (Lithium Triniobate), is found after annealing at 800°C. The presence of this additional peak, indicated by the black arrow, attests the deterioration of LN substrate as it is consequent of the dissociation reaction [26]:

$$3LiNbO_3 \rightarrow LiNb_3O_8 + Li_2O$$

As reported in [14], this monoclinic phase precipitates epitaxially at the surface of LN Z-cut substrate with $(20\bar{6})$ growth plane. Its thickness depends of the annealed temperature, time and pressure, but can rise up to 140 nm for a similar experiment [19]. Such compound was not detected at lower annealing temperatures, differently to what observed in [26]. We attribute this discrepancy to either (i) a low percentage of $LiNb_3O_8$ phase below 800°C, (ii) a poor $LiNb_3O_8$ crystallization, (iii) or to the quality and composition of the used LN substrates, which may be different between suppliers and lead to different deterioration temperatures [26, 27].

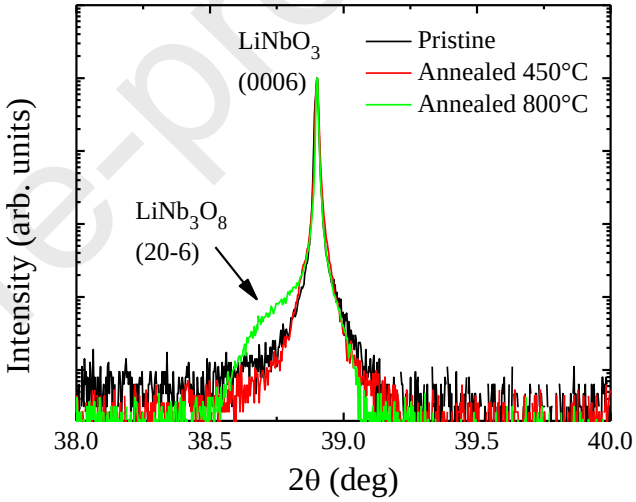

Figure 1. *θ-2θ X-ray diffraction scans measured on 10 nm thick Fe deposited on pristine LNZ (black), annealed 1 hour at 450 °C (red) and 800°C (green).*

3. Magnetic characterizations of Fe thin films

The magnetic characterization of the LN/Fe sample was performed with *in-situ* longitudinal MOKE measurement in the NFFA UHV MBE-cluster setup [29]. Measurements were done at room temperature using a *s*-polarized blue laser (435 nm) and chopper modulation at 789 Hz, with a laser spot size of about 500 μm^2 [29, 30]. The sample was rotated around its plane axis with steps of 45° to characterize its anisotropic response along the LN crystallographic directions H // LN [$\mathbf{11\bar{2}0}$], H // LN [$\mathbf{11\bar{2}0}$] + 45° and H // LN [$\mathbf{1\bar{1}00}$] directions.

In Figure 2 (a), (b), (c) and (d), the hysteresis loops along these directions are shown for the as-grown, annealed at 450°C, 600°C and 800°C Fe respectively. The hysteresis loops measured for annealing steps below 450°C did not

present any evolution in the magnetic behavior compared to the as-grown one (not shown). An additional polar plot of the in-plane coercive field is presented in inset of the Figure 1 (a).

4. Surface and volume chemistry characterizations

In order to understand the origin of the magnetic changes of Fe as a function of the annealing temperature, and to

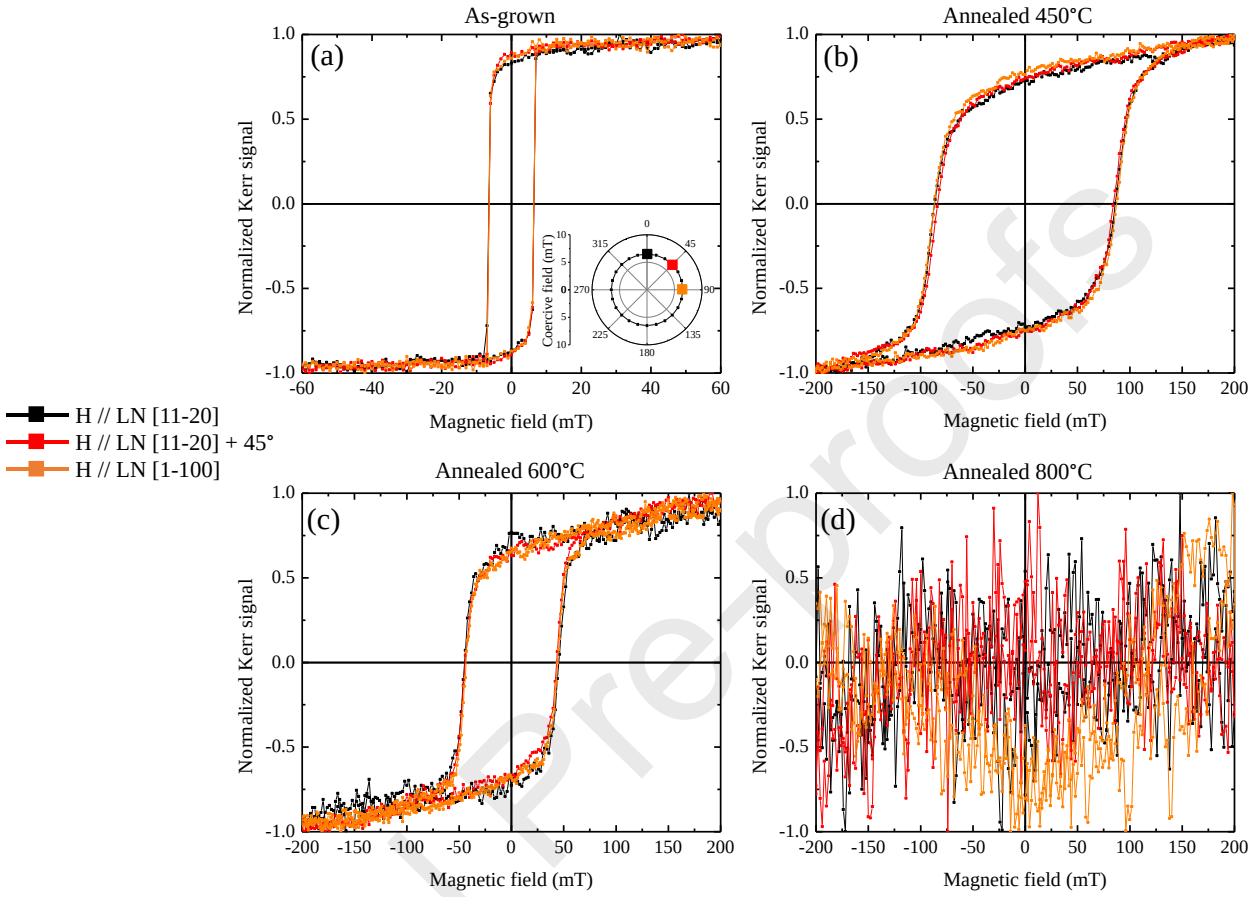

Figure 2. *Room temperature hysteresis loops measured for 10 nm thick Fe film deposited on pristine LNZ substrate before (a) and after annealing at 450 °C (b), 600°C (c), 800°C (d) along different crystallographic axis. A polar plot of the in-plane coercive field is present in inset of (a). The three colored squares correspond to the in-plane directions presented on the hysteresis loops.*

The following conclusion can be drawn from the above measurements:

(i) The Fe layer displays a perfectly in-plane isotropic behavior, with squared hysteresis loops for all sample conditions. This is consistent with a disordered polycrystalline growth of Fe, with no induced interfacial effects affecting the anisotropy [31].

(ii) The as-grown sample has a relatively low coercive field (6.5 mT), as expected for a soft magnetic material, but after annealing at 450°C the coercive field increases by an order of magnitude, reaching up to 85 mT, (*i.e.* 13 times larger). In addition, a linear slope appears after switching the magnetization, which remains up to 500 mT, without reaching a proper magnetic saturation of the hysteresis loop.

(iii) At 600°C, linear slopes are still present, while the coercive field reduces to 44 mT.

(v) At 800°C, no magneto-optical order was detected.

correlate them with the different ratios of phase decomposition of LN upon annealing, we performed a series of *in-situ* XPS and *ex-situ* XAS measurements at the different annealing steps.

XPS measurements were performed with an Al source (K_α = 1486.7 eV) and hemispherical electron energy analyzer in a dedicated chamber of the NFFA UHV MBE-cluster system [32]. Photoemission spectra were taken with the sample surface at 45° with respect to the incident beam. In this condition, the probed area on the sample surface covers an area of ~1 mm^2. One must note that the probing depth of such measurements is around 1 nm. All spectra were aligned with reference to the binding energy of C 1s peak.

Figure 3 presents a comparison of the survey scans between as-grown (black), annealed at 450 °C (red), 600 °C (blue) and 800 °C (green) panel (a) the Fe 2p core levels (b) and Nb 3d (c). Fitting of the core levels are also presented with the envelope and background respectively presented with solid

and dotted lines. For the sake of clarity, only Fe 2p as-grown core levels is shown.

with data from the literature [33-36], the binding energy of the measured Nb 3d peaks corresponds to the 5+ oxidization

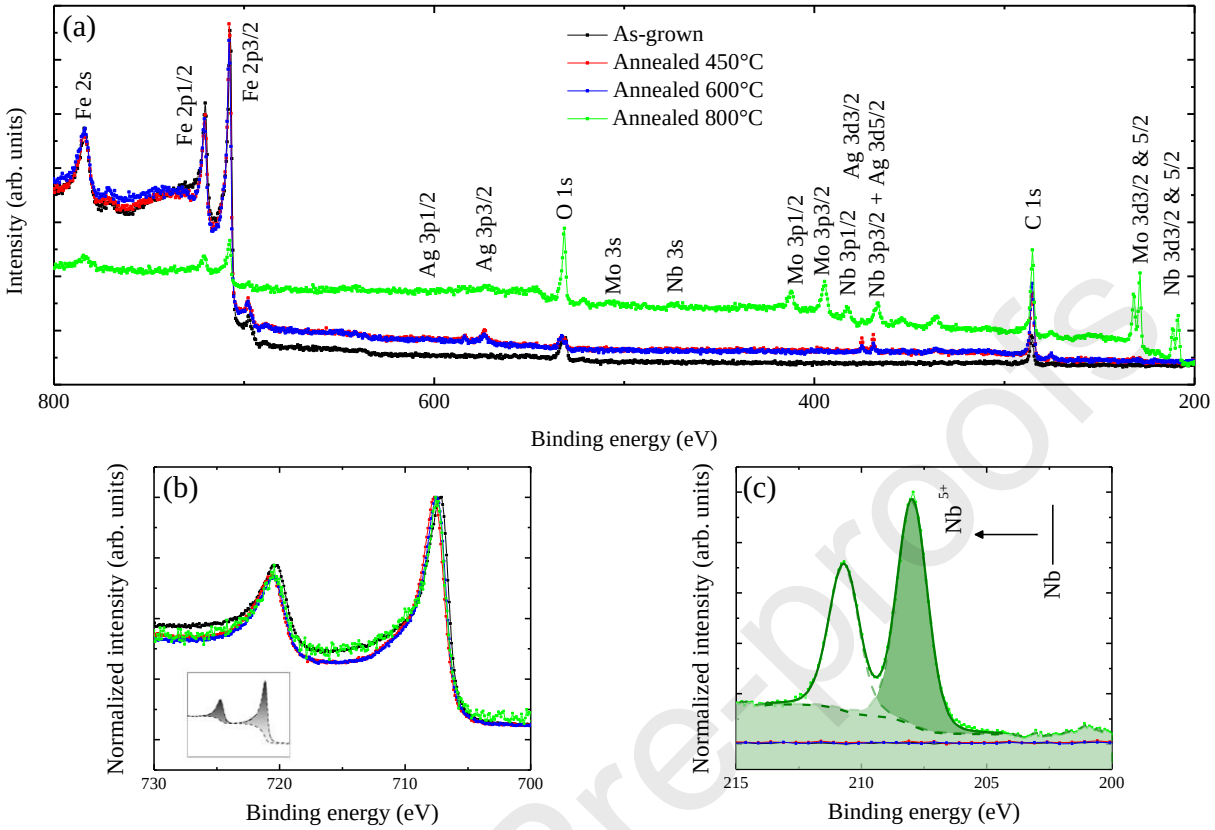

***Figure 3**. XPS survey and core level scans using Al source and respectively a pass energy of 40 and 30 eV. In (a), black, red, blue and green curves correspond respectively to as-grown, annealed at 450°C, 600°C and 800°C. Using the same color legend but renormalized to the main edges, Fe 2p and Nb 3d core levels are presented in (b) and (c) respectively. In addition, fitting of the core levels (asymmetric Doniach-Sunjic and symmetric Gaussian-Lorentzian line shapes for Fe and Nb respectively) plus their background (Shirley) are presented with solid and dotted lines respectively.*

The as-grown Fe layer spectrum presents Fe 2p peaks with the typical skewed lineshape of the metallic Iron. After the annealing at 450°C or 600°C, *i.e.* in correspondence of the large changes in magnetization (see Figures 2 (b) and (c)), the Fe 2p peaks and peakshape do not show appreciable changes (see Figure 3 (b)). This suggests that the large magnetic effects upon annealing are to be connected with modifications at the LN/Fe interface. A very small surface contamination coming from silver paste degassing during the annealing can be seen (see Ag 3d peaks close to 570 and 370 eV in Figure 3 (a)).

After annealing at 800°C, *i.e.* at the step at which no magnetic signal was recorded with MOKE, major changes appear in the XPS survey spectrum:

(i) The presence of Nb peaks, together with the increase of the O 1s contribution, is a sign of deterioration of the LN substrate, with dissociation species diffusing from the interface [18] towards the Iron surface. The Nb 3d symmetric peak shapes (Figure 3 (c)) are reminiscent of Nb oxides [33, 34]. After an analysis of the core levels and a comparison state and more especially to $LiNb_3O_8$ compound, slightly shifted from Nb_2O_5 and $LiNbO_3$. The Li 1s peak was indeed found at lower binding energy (not shown).

(ii) As a consequence of the interdiffusion between substrate elements and Iron overlayer, the intensity of the Fe 2p peaks is attenuated, but the lineshape remains metallic (see Figure 3 (b)).

(iii) The presence of Mo 3d peaks is due to impurities from the electron bombardment on the sample holder. From the analysis of the core levels weighted by their scattering cross sections (not shown), the Mo percentage is close to the one of Nb.

XAS measurements in Total Electron Yield (TEY) mode probes about ~ 5 nm of material below the surface. In order to reached the LN/Fe interface region, two samples of 5 nm Fe thick have been deposited on pristine LN and annealed at 450 °C and 800 °C. From the magnetic point of view, no significant differences were recorded with respect to the 10 nm thick case (Figure 2). The samples were then capped at RT with a 3 nm thick Au layer before exposure to

air. Once again, the deposition has been made by vapor phase epitaxy at a pressure not exceeding 1.10^{-9} mbar. Such process allowed transferring it from the growth chamber to APE-HE beamline [37]. XAS spectra at Fe $L_{2,3}$ edges were probed at room temperature, in linear polarization, with the sample surface at 45° with respect to the incident beam, normalizing at each energy value the intensity of the sample current to the incident photon flux current, probing an area of ~150 μm^2. The resulting spectra are shown in Figure 4. In addition, a metallic 5 nm Fe XAS reference spectrum (black curve) was added to help the comparison. The Fe reference sample was deposited and recorded in the same cluster setup and beamline, respectively.

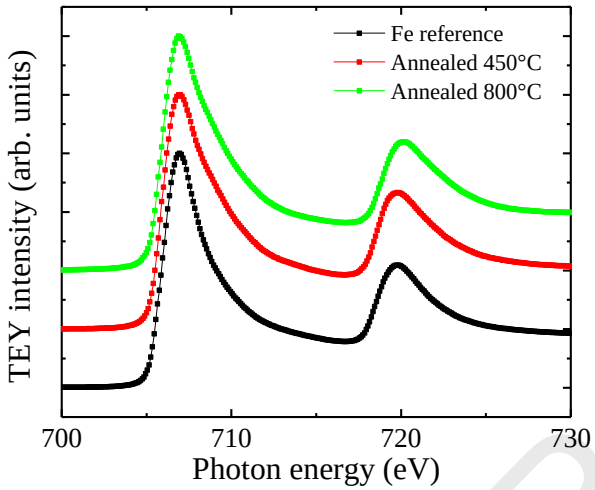

Figure 4. *Absorption spectra taking at Fe $L_{2,3}$ edges for a metallic Fe reference (black), a 5 nm thick Fe after annealing at 450 °C (red) and 800 °C (green).*

Quite surprisingly, for both annealing temperatures no visible changes from the metallic behavior (as the one of the Fe reference shown for comparison) are observed. This implies that no detectable chemistry changes are present through the whole Fe layer volume after LN annealing even at the 800°C step, which showed clear signs of LN phase decomposition up to the surface (Figure 3).

5. Microstructural variations

Since our measurements exclude chemical modifications of Fe upon annealing, we investigated the morphologic variations of LN/Fe after each annealing step. In order to do so, AFM images were recorded in tapping mode on 3 nm thick Au capped samples on 10 nm Fe thickness. Since Au capping layer was deposited after the annealing steps, we estimate that it does not affect substantially the observed morphology. Together with these AFM images, a possible scenario of the microstructural processes taking place during the annealing steps was derived and sketched in Figure 5.

The RMS roughness of the as-grown LN/Fe sample (Figure 5 (a)) is 0.8 ± 0.2 nm, which attests a relatively flat surface after room temperature deposition.

After annealing at 450°C (Figure 5 (b)), the RMS roughness dramatically increases up to 6.1 ± 0.2 nm, with the appearance of large spots on top of the surface. From our XPS characterizations (see Figure 3 (a) and (b)), we can consider that these features are still constituted by the metallic Fe top layer. Therefore, at this annealing step the increase of roughness due to the LN dissociation reaction, already observed in [27], has as direct consequence a modification of the morphology of the whole Fe thin film. The Fe layer evolves from a continuous flat film to a mix of continuous rough film and intermixed one, mainly close to the interface, with Li and Nb oxides clusters. We attribute such rich morphology as a possible reason of both the increase of the in-plane coercive field, due to the higher density of blocking points during the magnetization reversal [38-40], and of the linear slopes at high magnetic field, due to some domains that cannot be switched in this applied field range. Finally, the random distribution of these features in the AFM image is in accordance with the magnetic isotropy shown in Figure 2 (b).

The final AFM characterization after 800°C annealing (Figure 5 (c)) shows a reduction of the RMS roughness to 4.3 ± 0.2 nm, with a decrease of the clusters coverage. From literature, a decrease of the LN roughness is expected around 600-700°C [27, 36, 41]. This decrease is explained by a rearrangement of the top surface and of a part of the surface

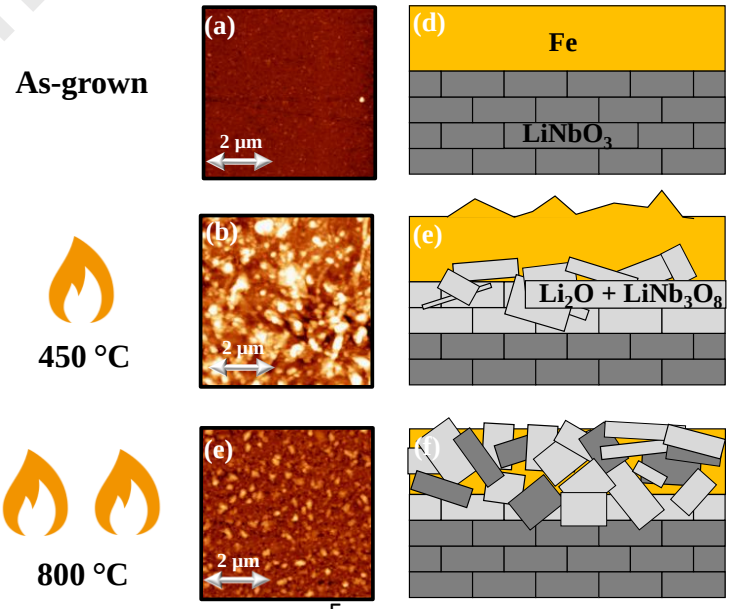

Figure 5. *Sketches and AFM top view images using tapping mode of the LN/Fe sample from as-grown Fe (a and d), annealed over 450°C (b and e) and at 800°C (c and f). Each cases possess its own color legend corresponding to the surface height. Yellow, dark and light grey colors correspond to Fe, LN and deteriorated substrate respectively.*

precipitates, as evidenced by the $LiNb_3O_8$ diffraction peak still present in XRD characterizations, and including possibly Fe in the present case, which is absorbed via a retransformation to the $LiNbO_3$ phase, as one can see from reduced Fe peaks in XPS characterizations. This second morphological transitions may explain therefore the decrease of the in-plane magnetic coercive field observed in Figure 2 (c) at 600°C. Increasing the annealing temperature up to 800°C may thus lead to a total transformation of the Fe thin film into dispersed clusters where no more magnetic response is recorded. Such dispersed clusters are however closely packed since additional EDS measurements (not shown here) using a scanning electron microscope setup revealed both Nb and Fe elements uniformly distributed over the whole probed area, taking into account a lateral resolution of about 150-200 nm.

6. Conclusion

In this work, we have studied LN/Fe samples deposited by vapor phase epitaxy as a function of post thermal annealing treatments. A full structural, magnetic, chemical and morphological characterization have been performed by means of XRD, MOKE, XPS, XAS and AFM measurements. The as-grown sample displays a ferromagnetic isotropic response with a squared hysteresis. Only starting from a post annealing temperatures of 450 °C or more, we found large modifications of the magnetic properties of the Fe layer. The coercive field increases up to a factor 13. This modification can be tuned according to the annealing temperature, which makes this process suitable for tailoring the magnetic coercivity of the magnetic layer over one order of magnitude span. The combination of XPS and XAS measurements showed that the LN phase decomposition does not induce any change in the chemical properties of the Fe layer, even after losing any appreciable magnetic response. From XRD measurements, we have observed the formation of a new crystallographic phase of the LN while the AFM measurements show that this transition is accompanied by large changes in the morphology of LN/Fe visible in the changes of the surface roughness and appearance and disappearance of clusters. We attribute the origin of the magnetic changes in the magnetic overlayer to partial decomposition of the substrate and release of diffusing species, *i.e.* stable Li and Nb oxides clusters, through the Fe thin film.

The role of the morphological changes upon LN annealing opens the way to further explore different LN/ferromagnetic interfaces, either with different LN-cuts or compositions (for example congruent [42], where the presence of defects is strongly reduced), or by substituting Fe with different ferromagnetic layers to tune the magnetic variations.

Acknowledgements

This work has been performed in the framework of the Nanoscience Foundry and Fine Analysis (NFFA-MIUR Italy Progetti Internazionali) facility.

References

[1] S. Andrieu, T. Hauet, M. Gottwald, A. Rajanikanth, L. Calmels, A. M. Bataille, F. Montaigne, S. Mangin, Z. Otero, P. Ohresser, P. Le Fèvre, F. Bertran, A. Resta, A. Vlad, A. Coati, Y. Garreau, Phys. Rev. Mat. **2** (2018) 064410.

[2] T. Vemulkar, J. Mansell, D. C. M. C. Petit, R. P. Cowburn, M. S. Lesniak, App. Phys. Lett. **107** (2015). 012403.

[3] S. Lakshmanan, S. K. Rao, M. R. Muthuvel, G. Chandrasekaran, H. A. Therese, J. of Magn. and Magn. Mat. **435** (2013) 81-86.

[4] C. M. Lee, L. X. Ye, H. K. Chen, T. H. Wu, IEEE. Tans on Magn. **49** (2013) 7.

[5] J. M. Hu, L. Q. Chen, C. W. Nan, Adv. Mater**. 28** (2016) 15.

[6] R. O. Cherifi, V. Ivanovskaya, L. C. Phillips, A. Zobelli, I. C. Infante, E. Jacquet, V. Garcia, S. Fusil, P. R. Briddon, N. Guiblin, A. Mougin, A. A. Unal, F. Kronast, S. Valencia, B. D. Dkhil, A. Barthélémy, M. Bibes, Nat. Mater**. 13** (2014) 345.

[7] S. Zhang, Y. G. Zhao, P. S. Li, J. J. Yang, S. Rizwan, J. X. Zhang, J. Seidel, T. L. Qu, Y. J. Yang, Z. L. Luo, Q. He, T. Zou, Q. P. Chen, J. W. Wang, L. F. Yang, Y. Sun, Y. Z. Wu, X. Xiao, X. F. Jin, J. Huang, C. Gao, X. F. Han, R. Ramesh, Phys. Rev. Lett**. 108** (2018) 137203.

[8] G. Vinai, F. Motti, V. Bonanni, A. Y. Petrov, S. Benedetti, C. Rinaldi, M. Stella, D. Cassese, S. Prato, M. Cantoni, G. Rossi, G. Panaccione, P. Torelli, Adv. Elec. Mat**. 5** (2019) 1900150.

[9] F. Motti, G. Vinai, A. Y. Petrov, B. A. Davidson, B. Gobaut, A. Filippetti, G. Rossi, G. Panaccione, P. Torelli, Phys. Rev. B**. 97** (2018) 094423.

[10] L. K. E. B. Serrona, R. Fujisaki, A. Sugimura, T. Oku da, N. Adachi, H. Ohsato, I. Sakamoto, A. Nakanishi, M. Motokawa, D. H. Ping, K. Hono, J. of Magn. and Magn. Mat. **260** (2003) 406-414.

[11] S. S. Mukherjee, F. Bai, D. MacMahon, C. L. Lee , S. K. Gupta, S. K. Kurinec, J. of App. Phys. **106** (2009) 033906.

[12] O. Sanchez-Dena, C. J. Villagomez, C. Fierro-Ruiz, A. S. Padilla-Robles, R. Farias, E. Vigueras-Santiago, S. Hernandez-Lopez, J. A. Reyes-Esqueda, Crystals. **9(7)** (2019) 340.

[13] M. Mignoni, PhD dissertation, Université de Metz (2010).

[14] X. Kang, L. Liang, W. Song, F. Wang, Y. Sang, H. Liu, Cryst. Eng. Comm**. 18** (2016) 8136.

[15] J. Bhatt, I. Bhaumik, S. Ganesamoorthy, R. Bright, M. Soharab, A. K. Karnal, P. K. Gupta, Crystals**. 7(2)** (2017) 23.

[16] M. Rusing, P. O. Weigel, J. Zhao, S. Mookherjea, IEEE. Nanot. Mag**. 13** (2019) 2916115.

[17] C. K. Campbell, book Surface Acoustic Wave Devices for Mobile and Wireless Communications, San Diego, California: Academic Press (1998).
[18] V. Polewczyk, K. Dumesnil, D. Lacour, M. Moutaouekkil, H. Mjahed, N. Tiercelin, S. Petit-Watelot, Y. Dusch, S. Hage-Ali, O. Elmazria, F. Montaigne, A. Talbi, O. Bou Matar, M. Hehn, Phys. Rev. App. **8** (2017) 024001.
[19] V. Polewczyk, PhD dissertation, Université de Lorraine (2018).
[20] M. Yamaguchi, K. Y. Hashimoto, H. Kogo, M. Naoe, IEEE. Trans. Magn. **16** (1980).
[21] M. Elhosni, O. Elmazria, S. Petit-Watelot, L. Bouvot, S. Zhgoon, A. Talbi, M. Hehn, K. Ait Aissa, S. Hage-Ali, D. Lacour, F. Sarry, O. Boumatar, Sensors and Actuators A: Physical**. 240** (2016) 41-49.
[22] K. Matsubara, P. Fons, A. Yamada, M. Watanabe, S. Niki, Thin Solid Films**. 347** (1999) 238-240.
[23] M. H. Nam, W. Yang, M. D. Kim, I. S. Park, Journal of the Korean Physical Society**. 58** (2011) 5.
[24] M. Kadota, S. Ito, Y. Ito, T. Hada, K. Okaguchi, Jpn. J. Appl. Phys**. 50** (2011) 07HD07.
[25] M. Weiler, L. Dreher, C. Heeg, H. Huebl, R. Gross, M. S. Brandt, S. T. B. Goennenwein, Phys. Rev. Lett. **106** (2011) 117601.
[26] G. Namkoong, K. K. Lee, S.M. Madison, W. Henderson, S. E. Ralph, W. A. Doolittle, Appl. Phys. Lett. **87** (2005) 171107.
[27] H. Nagata, K. Shima, J. Ichikawa, J. Am. Ceram. Soc. **80** (1997) 1203-207.
[28] N. Chowdhury, S. Bedanta, AIP Advances**. 4** (2014) 027104.
[29] G. Vinai, F. Motti, A. Y. Petrov, V. Polewczyk, V. Bonanni, R. Edla, R. Ciprian, B. Gobaut, J. Fujii , A. Deluisa, D. Benedetti, F. Salvador, A. Fondacaro, G. Rossi, G. Panaccione, B. A. Davidson, P. Torelli, Review of scientific Instruments (2020) Submitted manuscript.
[30] G. Vinai, B. Ressel, P. Torelli, F. Loi, B. Gobaut, R. Cianco, B. Casarin, A. Caretta, L. Capasso, F. Parmigiani, F. Cugini, M. Solzi, M. Malvestuto, R. Ciprian, Nanoscale**. 10** (2018) 1326.
[31] A. Yamaguchi, T. Ohkochi, A. Yasui, T. Kinoshita, K. Yamada, J. of Magn. and Magn. Mat. **453** (2018) 107-113.
[32] P. Torelli, M. Sacchi, G. Cautero, M. Cautero, B. Krastanov, P. Lacovig, P. Pittana, R. Sergo, R. Tommasini, A. Fondacaro, F. Offi, G. Paolicelli, G. Stefani, M. Grioni, R. Verbeni, G. Monaco, G. Panaccione, Rev. Sci. Instrum. **76** (2005) 023909.
[33] M. Aufray, S. Menuel, Y. Fort, J. Eschbach, D. Rouxel, B. Vincent, J. of Nano. and Nanot. **9** (2009) 4780-4785.
[34] H. Zhai, H. Liu, L. Zheng, C. Hu, X. Zhang, Q. Li, J. Yang, Nanoscale. Research. Letters. **12** (2017) 463.
[35] V. V. Atuchin, I. E. Kalabin, V. G. Kesler, N. V. Pervukhina, J. of Elec. Spec. and Rela. Phen. **142** (2005) 129-134.
[36] R. N. Zhukov, T. S. Ilina, E. A. Skryleva, B. R. Senatulin, I. V. Kubasov, D. A. Kiselev, G. Suchaneck, M. D. Malinkovich, T. N. Parkhomenko, A. G. Savchenko, J. Nano-Electron Phys. **10** (2018) 02009.
[37] G. Panaccione, I. Vobornik, J. Fujii, D. Krizmancic, E. Annese, L. Giovanelli, F. Maccherozzi, F. Salvador, A. De Luisa, D. Benedetti, A. Gruden, P. Bertoch, F. Polack, D. Cocco, G. Sostero, B. Diviacco, M. Hochstrasser, U. Maier, D. Pescia, C. H. Back, T. Greber, J. Osterwalder, M. Galaktionov, M. Sancrotti, G. Rossi, Rev. Sci. Instrum. **80** (2009) 043105.
[38] M. S. Pierce, C. R. Buechler, L. B. Sorensen, S. D. Kevan, E. A. Jagla, J. M. Deutsch, T. Mai, O. Narayan, J. E. Davies, K. Liu, H. G. Katzgraber, O. Hellwing, E. E. Fullerton, P. Fischer, J. B. Kortright, Phys. Rev. B. **75** (2007) 144406.
[39] J. Swerts, S. Vandezande, K. Temst, V. Haesendonck, Solid. State. Comm. **131** (2004) 359-363.
[40] M. Li, Y. P. Zhao, G. C. Wang, H. G. Min, J. of Appl. Phys. **83** (1998) 11.
[41] D. A. Kiselev, R. N. Zhukov, A. S. Bykov, M. I. Voronova, K. D. Shcherbachev, M. D. Malinkovich, Y. N. Parkhomenko, Inor. Mater. **50** (2014) 419.
[42] J. Streque, T. Aubert, N. Kokanyan, F. Bartoli, A. Taguett, V. Polewczyk, E. Kokanyan, S. Hage-Ali, P. Boulet, O. Elmazria, IEEE. Sensors. Letters. **3** (2019) 4.

- Ion migration due to thermal annealing
- Dissociation reaction in ferroelecric substrate
- Change of morphology
- Tuning of magnetic coercivity
- Defects induced in magnetic thin films

V. Polewczyk : Main investigation
G. Vinai : Investigation + Writing + Validation
F. Motti : Investigation + Writing + Validation
S. Santhosh : Investigation
S. Benedetti : Investigation + Writing + Validation
G. Rossi : Investigation + Writing + Validation + Funding acquisition
P. Torelli : Investigation + Writing + Validation + Project administration + Conceptualization

Declaration of interests

☐ The authors declare that they have no known competing financial interests or personal relationships that could have appeared to influence the work reported in this paper.

☐The authors declare the following financial interests/personal relationships which may be considered as potential competing interests:

Vincent Polewczyk